KSCE Journal of Civil Engineering (2021) 25(4):1283-1294
DOI 10.1007/s12205-021-0959-z

pISSN 1226-7988, eISSN 1976-3808
www.springer.com/12205

Geotechnical Engineering

Shear Behavior of Marlstone Containing Parallel Fissure under Normal Unloading

Zhiming Yin[a], **Xinrong Liu**[a,b,c,d], **Zhongping Yang**[a,b,c], **and Yanlei Wang**[e]

[a]*School of Civil Engineering, Chongqing University, Chongqing 400045, China*
[b]*Key Laboratory of New Technology for Construction of Cities in Mountain Area, Chongqing University, Ministry of Education, Chongqing 400045, China*
[c]*National Joint Engineering Research Center for Prevention and Control of Environmental Geological Hazards in the TGR Area Chongqing University, Chongqing 400045, China*
[d]*State Key Laboratory of Coal Mine Disaster Dynamics and Control, Chongqing University, Chongqing 400044, China*
[e]*Chongqing Bureau of Geology and Minerals Exploration, Chongqing 401121, China*

ARTICLE HISTORY

Received 20 July 2020
Revised 23 October 2020
Accepted 12 November 2020
Published Online 29 January 2021

KEYWORDS

Normal unloading shear test
Parallel fissures
Failure pattern
Shear strength
Deformation

ABSTRACT

Shear tests under normal unloading were carried out to further study the shear mechanical behavior of marlstone containing parallel fissures. The results reveal that the failure on the rock bridge is tensile failure except for the limited extrusion failure at the tip of the prefabricated fissure. The failure on both sides is generally tensile-shear mixed failure, in which the tensile failure is mainly concentrated in the middle of both sides. In general, it can be summarized as a tensile-shear failure mode of STS-T-STS (S means shear failure, T means tension failure). The failure normal stress of the specimens gradually increases and then decreases with the increase of the fissure inclination, increases with an increase in the initial normal/shear stress, and decreases with the increase of the unloading rate. Strong dilation occurred in the shear process of the specimens, which shows obvious arch effect. The variation law of dilatancy deformation and horizontal deformation in the stage of normal stress unloading is just opposite to that of the failure normal stress. The increasing effect of high shear stress on shear deformation is greater than that of dilatancy deformation, while the inhibiting effect of high normal stress on dilatancy deformation is greater than that of the shear deformation.

1. Introduction

Discontinuities such as faults, joints, and fractures widely exist in the high and steep rock slope, especially in the karst slope (Fig. 1). These discontinuous interfaces usually appear in groups with similar directions and features (Gratchev et al., 2016; Zhang et al., 2019; Zhang and Zhou, 2020), forming potential discontinuity sliding surface, which plays an important role in the stability of the slope (Hoek, 1983; Guo and Qi, 2015; Zhao et al., 2019).

Engineering practices show that the instability of many rock slopes was caused by the fracture propagation and finally coalescence of rock bridge between discontinuities (Terzaghi, 1962; Eberhardt et al., 2004; Huang and Qi, 2017), such as the step-path failure of Aishihik river bank slope in Canada (Brideau et al., 2009), the 1991 Randa rockslide which slide along discontinuous interface (Eberhardt et al., 2004), the instability of the Malpasset Dam in France (Post and Bonazzi, 1987), and the Nayong landslide in China (Xiao et al., 2018a). The failure of these rock slopes was caused by natural disturbances (such as the actions of gravity and weathering, and the erosion of surface water and river) or human engineering activities (such as the slope excavation and underground mining), with a common mechanical properties of unloading (Fig. 2). In many cases, rocks fail due to shear under unloading normal stress. Due to the unloading of normal stress, the shear strength of potential sliding surface decreases, and natural discontinuities are more likely to be connected through a complete rock bridge, resulting in shear fracture of slope rock mass (Zhong et al., 2020). Owing to discontinuity and heterogeneity, the mechanical behaviors of rock under loading and unloading conditions are very different.

CORRESPONDENCE Zhongping Yang ✉ yang-zhp@163.com ✉ School of Civil Engineering, Chongqing University, Chongqing 400045, China; Key Laboratory of New Technology for Construction of Cities in Mountain Area, Chongqing University, Ministry of Education, Chongqing 400045, China; National Joint Engineering Research Center for Prevention and Control of Environmental Geological Hazards in the TGR Area Chongqing University, Chongqing 400045, China

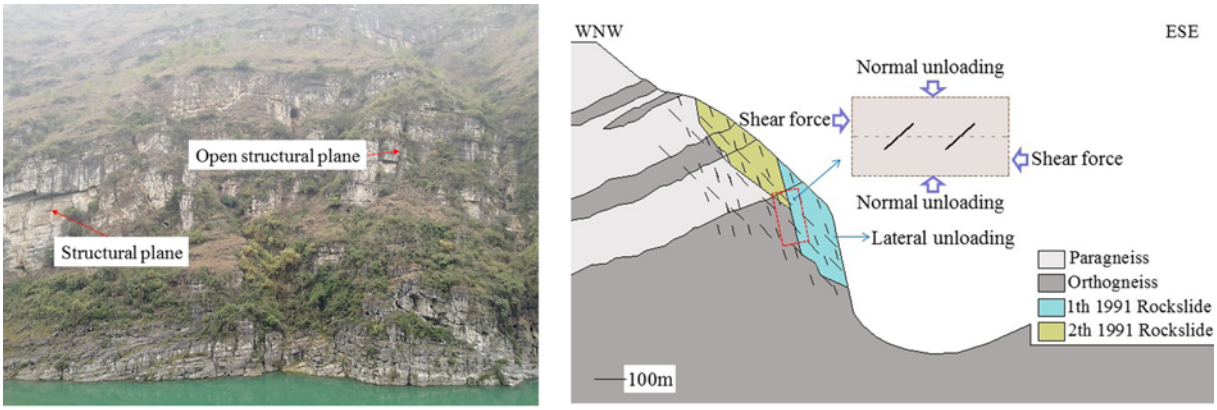

Fig. 1. Examples of Slope with a Large Number of Joints and Fissures: (a) A Karst Slope of a River Bank in Wulong, Chongqing, China, (b) Geological Section of the 1991 Randa Rockslide (Eberhardt et al., 2004)

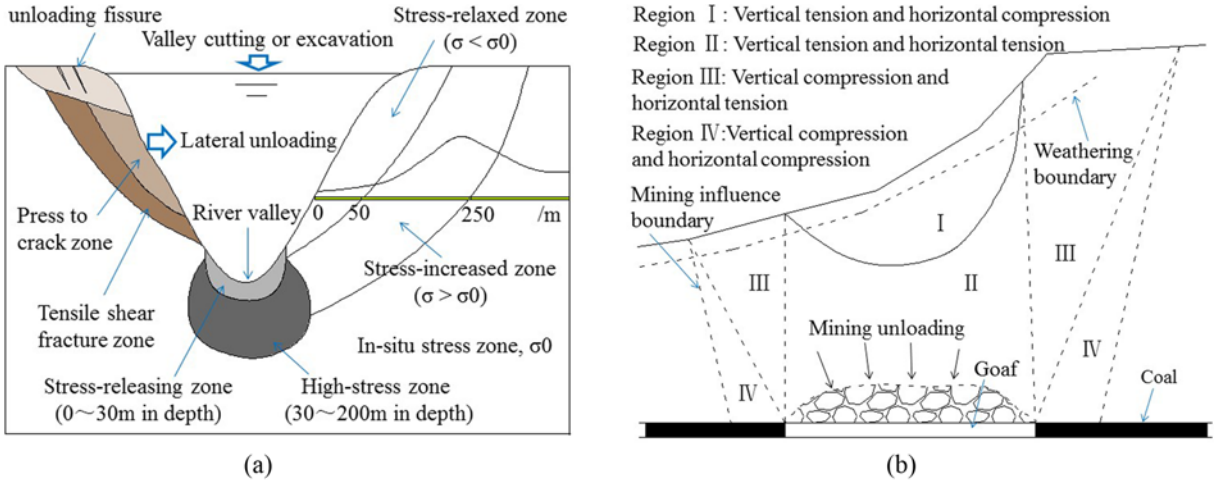

Fig. 2. Unloading of Slope Rock Mass Caused by Valley Cutting or Excavation: (a) Unloading Caused by Valley Cutting or Slope Excavation (Huang, 2008), (b) Unloading Caused by Underground Mining (Tang, 1989)

Therefore, it is necessary to reveal the shear mechanical behavior of fissured rock mass under unloading conditions.

Abundant researches have been performed on the unloading behavior of the fissured rock mass (Xie and He, 2004; Yang et al., 2008; Liu, 2012; Huang and Huang, 2014; Xiao et al., 2018b). Most of these studies used triaxial unloading tests to investigate the effect of the unloading path on the deformation, strength and failure characteristics of the fissured rock mass. For the triaxial unloading test, the maximum shear stress on the potential failure surface increases gradually until compression shear failure occurs because the deviatoric stress increases during unloading confining stress. So the triaxial unloading test cannot directly and effectively model the shear failure mechanism of the fissured rock mass that has suffered only from unloading normal stress.

Direct shear tests under constant normal stress have been widely used as a common and effective way to investigate the shear mechanical behavior of the fissured rock mass (Lajtai, 1969; Wong et al., 2001; Wong and Wang, 2002; Gehle and Kutter, 2003; Yin et al., 2020). Obviously, the direct shear tests cannot reveal shear failure of the fissured rock mass during unloading of normal stress, as the normal stress remains unchanged throughout the direct shear tests. Rock masses in slopes are subjected to shear-normal stress, after surface excavation, the normal stress is decreasing continuously. If unstable, the lower parts of slopes generally experience shear fracture, which is a very common failure pattern in the excavation engineering of the geological body. However, thus far, the shear mechanical properties of the fissured rock mass under normal unloading are rarely studied, and even less on Marlstone. Zhong et al. (2020) carried out normal unloading shear tests to study the shear failure behavior of red-sandstone containing a parallel fissure pair. It observed four failure modes of rock bridge: tensile failure, tensile-shear failure, shear failure and two-stage failure, according to the length and inclination range of rock bridge, summarized the failure rules of rock bridge, and investigated the strength and deformation behavior. However, the effect of unloading rate didn't be considered in this study. And the influence of bending moment caused by the shear force in the calculation of stress on

the fracture surface of the element didn't be considered neither. Meanwhile, the mechanical properties of red-sandstone and marlstone are quite different.

Therefore, in this study, normal unloading shear tests were carried out to investigate the shear mechanism of marlstone containing parallel fissures under different fissure inclination, initial normal stress, initial shear stress, and normal unloading rate. The test element (Fig. 1(b)) simplifies the stress states found in a jointed rock slope under surface excavation (Eberhardt et al., 2004). Tests process includes three steps: Firstly, loading the normal force to a target value (called initial normal stress); Secondly, after the normal force loading is stable, keep the normal force unchanged, and then loading the shear force to a target value (called initial shear stress); And finally, keep the shear force unchanged and unload the normal force until the specimen failed. According to the fracture morphology and stress state of the rock bridge, the failure patterns and fracture mechanism of rock specimens with different fissure inclinations under different initial normal and shear stresses were analyzed, and the strength and deformation behavior were investigated. The differences of the findings between loading shear tests and unloading shear tests, and those between the current study and previous studies are discussed.

2. Experimental Study

2.1 Rock Specimen Preparation

In this study, hard brittle marlstone of stratum T_1^y from the Zhangjiawan landslide site in Guizhou, China, were used. The values of the density, Yong's modulus, Poisson's ratio, uniaxial compressive strength, tensile strength, cohesion, and internal frictional angle are 2.71 g/cm³, 27 GPa, 2.27, 92 MPa, 5.6 MPa, 2.52 MPa, and 39°, respectively. Considering the dimensional requirements of GB/T 50266-2013 (2013) and the thickness limitation for cutting of rock by the water jet cutter, the specimen was designed as a cuboid, with a size of 100 mm × 60 mm × 40 mm. The length and spacing of the prefabricated fissures are 20 mm and 40 mm respectively, and the center of the prefabricated fissure is fixed on the symmetry plane of the specimen. The fissure inclination α of the specimen is a geometric variable.

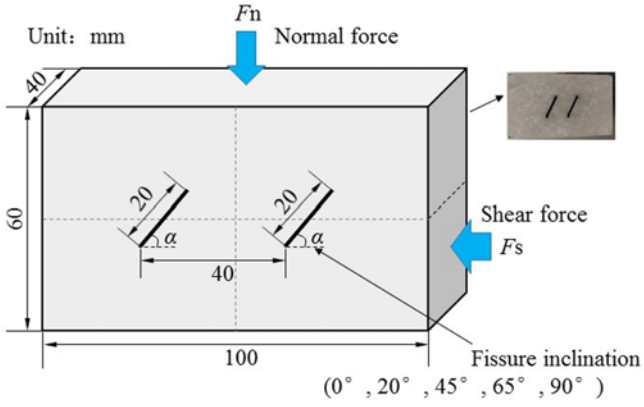

Fig. 3. Geometrical Dimension of Specimen

The processing of the specimen includes three steps: cutting of rock block by rock cutter, Grinding of the specimen surface by grinding wheel and rock grinder, and cutting of prefabricated fissure by high-speed water cutter. The specimen dimension deviation, verticality deviation and the prefabricated fissure opening are controlled within 0.2 mm, 0.2°, and 2 mm, respectively. The geometrical dimension of the specimen was illustrated in Fig. 3.

2.2 Testing System

The tests were performed in an electro-hydraulic servo rock shear testing machine (WDAJ-600), as shown Fig. 4. Tests process includes three steps: Firstly, loading the normal force to a target value (σ_1); Secondly, after the normal force loading is stable, keep the normal force unchanged, and then loading the shear force to a target value (τ_1); Finally, keep the shear force unchanged and unload the normal force until the specimen failed (The failure normal stress is named σ_2). All of the loading and

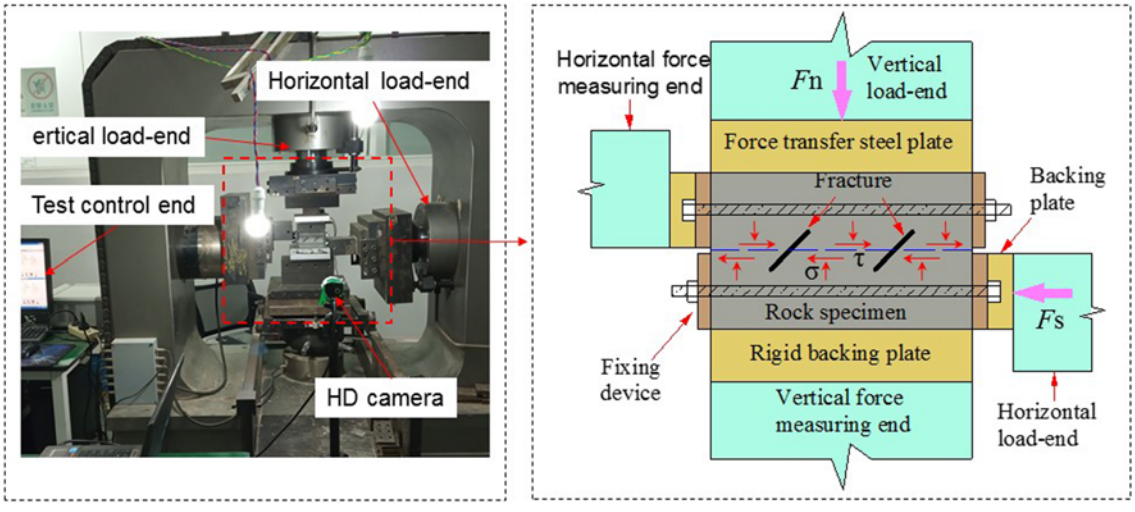

Fig. 4. Layout of the Test System

Table 1. Test Groups of the Rock Specimens

Test group	Specimen number	Fissure inclination, α (°)	Initial normal stress, σ_1 (MPa)	Initial shear stress, τ_1 (MPa)	Unloading rate, v (kN/s)
Group A	A0, A20, A45, A65, A90	0, 20, 45, 65, 90	12	8	0.15
Group B	B7, B8, B9, B10	45	12	7, 8, 9, 10	0.15
Group C	C8, C10, C12	45	8, 10, 12	8	0.15
Group D	D12, D15, D18	45	12	8	0.12, 0.15, 0.18

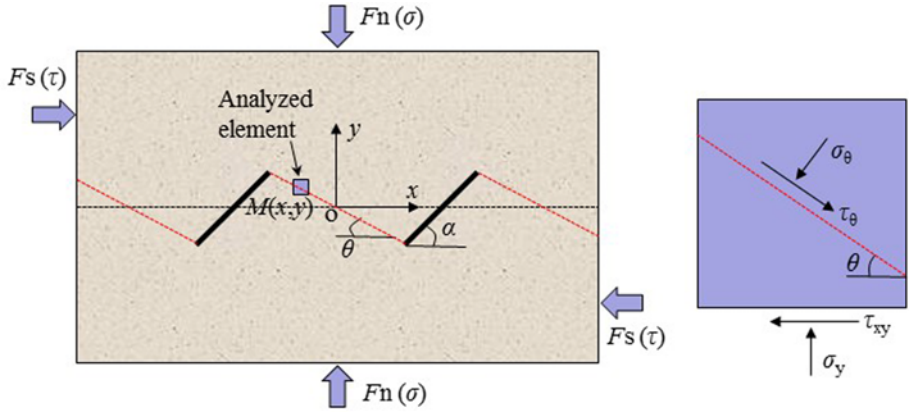

Fig. 5. The Stress State of the Square Element on Failure Surface: (a) The Stress State of the Specimens, (b) The Stress State of the Analyzed Element

unloading rates are 0.15 kN/s. In order to ensure that the shear force can be transferred to the shear plane, the specimen is fixed with an auxiliary device. The specimen should be aligned with the vertical and horizontal loading heads to prevent deviation during shearing. In addition, high-resolution camera was used to record the cracking behavior and shear failure process of the specimen during shear tests.

2.3 Test Groups

In the tests, four influencing factors were considered, namely, the fissure inclination (α), initial normal stress (σ_1), initial shear stress (τ_1), and normal unloading rate (v). According to the different geometry and loading conditions, the tests were divided into four groups as shown in Table 1.

A20 is the specimen number with fissure inclination of 20°; B7 is the specimen number with an initial shear stress of 7 MPa; C8 is the specimen number with the initial normal stress of 8 MPa; D15 is the specimen number with a normal unloading rate of 0.15 kN/s.

3. Experimental Results and Analysis

3.1 Failure Features

By replaying the photos of the test processes, the crack initiation and coalescence process of rock specimen can be observed clearly, and the crack properties can be determined preliminarily. The shear failure surface is often accompanied by white shear and extrusion scratches, shear debris and shear fracture zone, while the tensile fracture section is often rough and gray and without white rock powder. So the shear failure degree ζ (the area of the shear scratch to the total area of fracture surface) was defined and calculated to further analyze the failure characteristics of the specimens.

Besides, the shear fracture characteristics of the specimen also can be studied by analyzing the stress state of the point on the rock bridge. The element $M(x, y)$ is affected by a normal stress σ_y and a shear stress $\tau_{xy,}$ as shown in Fig. 5. The normal stress σ_θ and shear stress τ_θ in the direction of the failure surface can be obtained by Eq. (1):

$$\begin{cases} \sigma_\theta = \dfrac{1+\cos 2\theta}{2}\sigma_y - \tau_{xy}\sin 2\theta \\ \tau_\theta = -\dfrac{\sin 2\theta}{2}\sigma_y - \tau_{xy}\cos 2\theta \end{cases} . \tag{1}$$

Considering the moment action of shear force on the specimen, a certain tensile stress σ_t is produced on the shear plane, which can be obtained by Eq. (2). σ_y and τ_{xy} can be obtained by Eq. (3). In Eq. (2), a is the length of the specimen, b is the height of the specimen, and c is the width of the specimen.

$$\sigma_t = \frac{\tau \cdot a \cdot c \cdot \dfrac{b}{4}}{a \cdot c \cdot \dfrac{a}{2}} = 0.3\tau \tag{2}$$

$$\begin{cases} \sigma_y = \sigma - \sigma_t \\ \tau_{xy} = \tau \end{cases} \tag{3}$$

In the following analysis, σ_θ and τ_θ refer to the average stress on the whole failure surface, which can be obtained by formula (1 − 3) in which $\sigma = \sigma_2$ (the failure normal stress) and $\tau = \tau_1$ (the

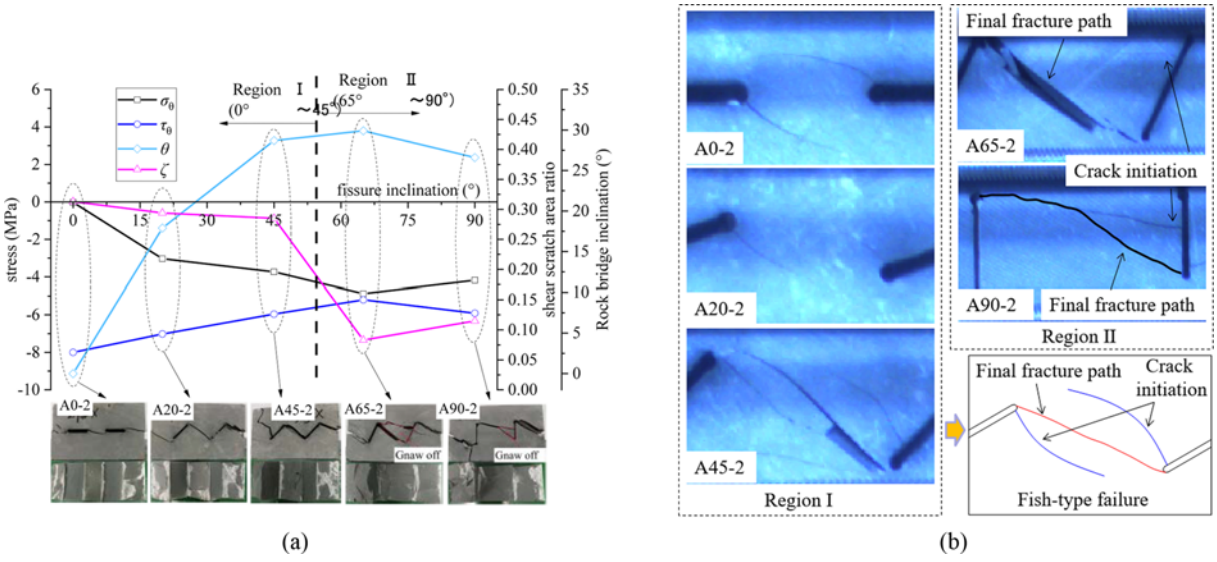

Fig. 6. The Failure Patterns of the Specimens with Different Fissure Inclinations: (a) The Failure Patterns of the Specimens, (b) The Failure Characteristics of Rock Bridge

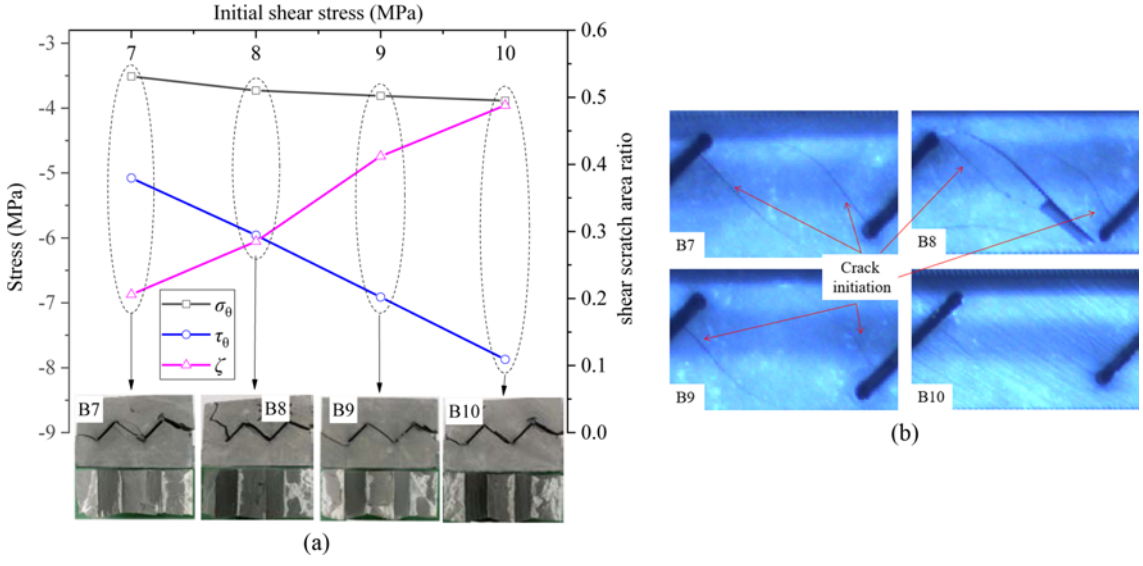

Fig. 7. The Failure Features of the Specimens with Different Initial Shear Stress: (a) The Failure Patterns of the Specimens, (b) The Failure Characteristics of Rock Bridge

initial shear stress). According to the geometric relationship, the relation curve of rock bridge inclination (θ) and fissure inclination (α) was obtained. With the increase of α, θ and σ_θ (tensile stress) increase first and then decrease, while τ_θ and ζ decrease first and then increase gently (Fig. 6). Therefore, it can be considered that the shear failure degree of the specimen increases with the decrease of bridge inclination. It can be seen from Fig. 6 that all the specimens are fractured approximately along the direction of the rock bridge. When α is small (region I), the initial crack position is close to the tip of the prefabricated fissure, and the fish-type failure appears in the rock bridge, while α is large (region II), the initial crack position is close to the middle of the prefabricated fissure, and the gnawing failure appears along the middle of the fissure. This is because the change of the fissure inclination changes the stress state of the failure surface, and eventually leads to the change in the failure mode of the specimen.

It can be seen from Fig. 7 that with an increase in the initial shear stress, σ_θ increases slowly, while τ_θ and ζ increase obviously, that is, the shear failure degree of the specimen increases. When the initial shear stress is less than 10 MPa, the fish-type failure appears in the rock bridge. Before fractured along the direction of the rock bridge, two wing cracks were found. When the initial shear stress is 10 MPa, apart from the crack along the direction of the rock bridge, no other cracks were found. It illustrates that the failure of the specimens under high shear stress is more sudden, and no local release of energy before shear fracture of specimens.

Figure 8 illustrates the influence of initial normal stress on the

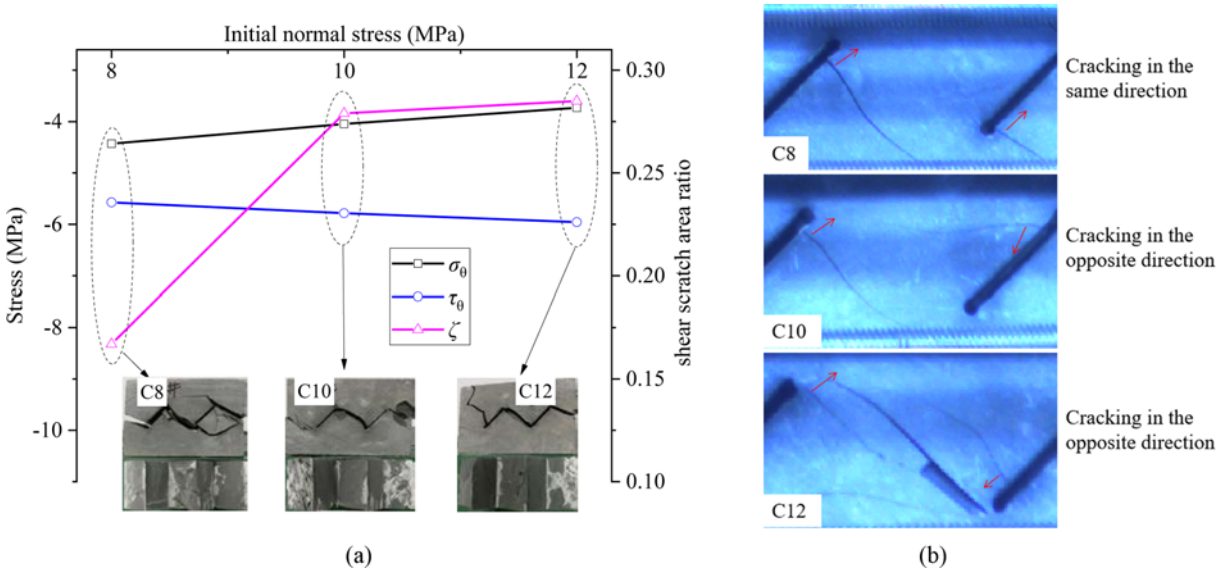

Fig. 8. The Failure Characteristics of the Specimens with Different Initial Normal Stress: (a) The Failure Patterns of the Specimens, (b) The Failure Characteristics of Rock Bridge

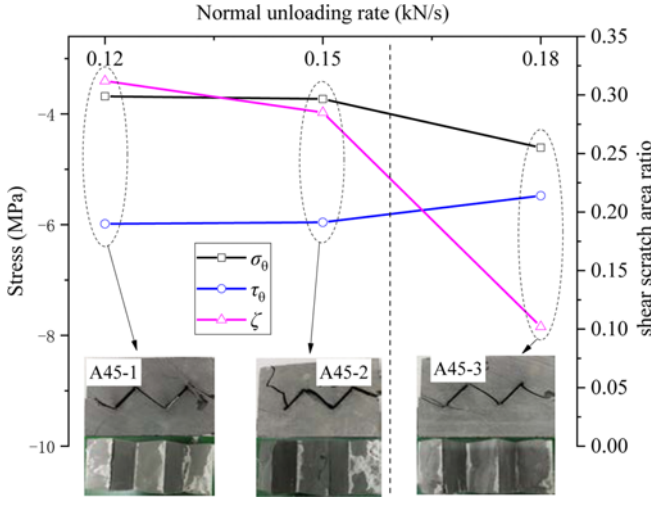

Fig. 9. The Failure Patterns of the Specimens with Different Unloading Rate

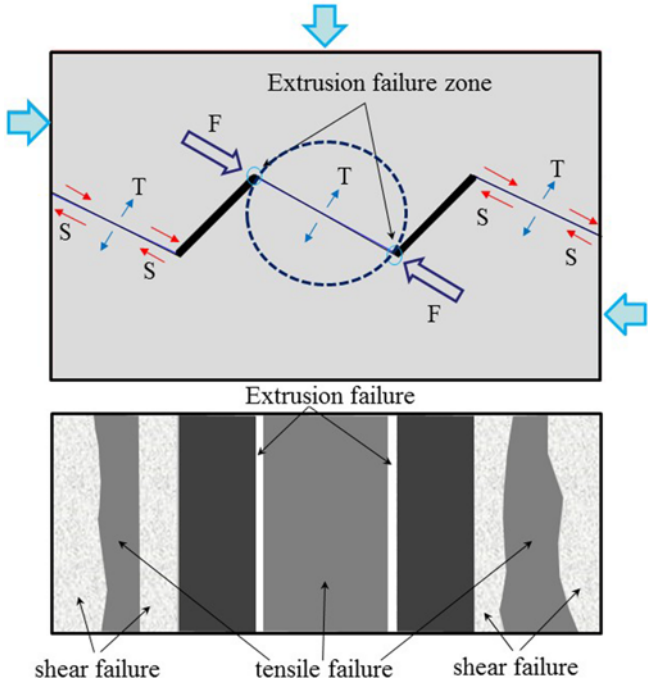

Fig. 10. Typical Failure Mode of the Specimens

failure pattern of the specimens. With the increase of the initial normal stress, σ_θ decreases, while τ_θ and ζ increase. The opening direction of the two initial tensile cracks is the same when the initial normal stress is 8 MPa, and gradually changes to the opposite direction when the initial normal stress increases from 8 MPa.

Figure 9 shows the failure characteristics of the specimens under different normal unloading rates with a fissure inclination of 45°, an initial normal stress of 12 MPa, and an initial shear stress of 8 MPa. It can be found from Fig. 9 that with the increase of normal unloading rate, σ_θ increases while τ_θ and ζ decrease, and the tensile failure characteristics become more obvious. When the normal unloading rate is 0.18 kN/s, the failure of the specimen section is almost all tensile failure.

It can be seen from Figs. 6 – 9 that the normal stress σ_θ of specimens is all tensile stress. Therefore, the failure surface of the specimens is mainly subjected to tensile and shear stress. With the decreases of σ_θ and increases of τ_θ, ζ increases. ζ of the specimens is all less than 0.5, which means that the tensile failure characteristics of the specimens are more obvious. However, the average tensile stress of the failure surface of the specimens is all in the range of 3 – 5 MPa, which is obviously less than the uniaxial tensile strength of intact rock. It indicates that the tensile strength under the mixed action of tension and shear is obviously less than that of uniaxial tensile strength. The failure on the rock bridge is tensile failure except for the limited extrusion failure at

the tip of the prefabricated fissure, which can be explained approximately by Brazilian splitting model, as shown in Fig. 10. The failure on both sides is generally tensile-shear mixed failure, in which the tensile failure is mainly concentrated in the middle of both sides. In general, it can be summarized as a tensile-shear failure mode of STS-T-STS, as shown in Fig. 10 (S for shear failure and T for tension failure). Because of the concentration of normal compressive stress at the fissure tip, the normal pressure at the fissure tip is greater than that in the middle of the rock bridge. And due to the non-uniformity of normal stress, strong dilation deformation occurred in the shear process of the specimens, which shows an obvious arch effect.

3.2 Strength Behaviors

The relationship between the failure normal stress (σ_2) and fissure inclination (α) under the same initial stress state was presented in Fig. 11(a). Under the same initial stress state, if σ_2 is large, it means that the specimen is easy to damage, namely the shear strength of the specimen is low. Overall, σ_2 gradually increases as α increases from 0° to 45° and reverses when α grows from 45° to 90°. This is because with the increase of α, the area of shear failure of the specimen decreases first and then increases slowly. Owing to the weak strength of rock in tension, the strength of the rock specimen with a fissure inclination of 45° is the lowest, and the strength of the rock specimen with a fissure inclination of 0° is the highest.

Figures 11(b) and 11(c) illustrated the relationship between the failure normal stress (σ_2) and the initial stress level. For Fig. 11(b), we can see that when σ_1 is the same, σ_2 increases linearly with the increase of τ_1. And through the linear fitting of the test curve, the relation between σ_2 and τ_1 is obtained. It can be seen from Fig. 11(c) that when τ_1 is the same, σ_2 increases slightly with the increase of σ_1. It is felt that the shear strength of the specimen decreases with the increase of the initial normal stress. This is because the duration of unloading is longer under the action of high normal stress, making the deformation more sufficient in the shear process.

Figure 11(d) shows the relationship between the failure normal stress (σ_2) and the normal unloading rate (υ) of the specimens (α

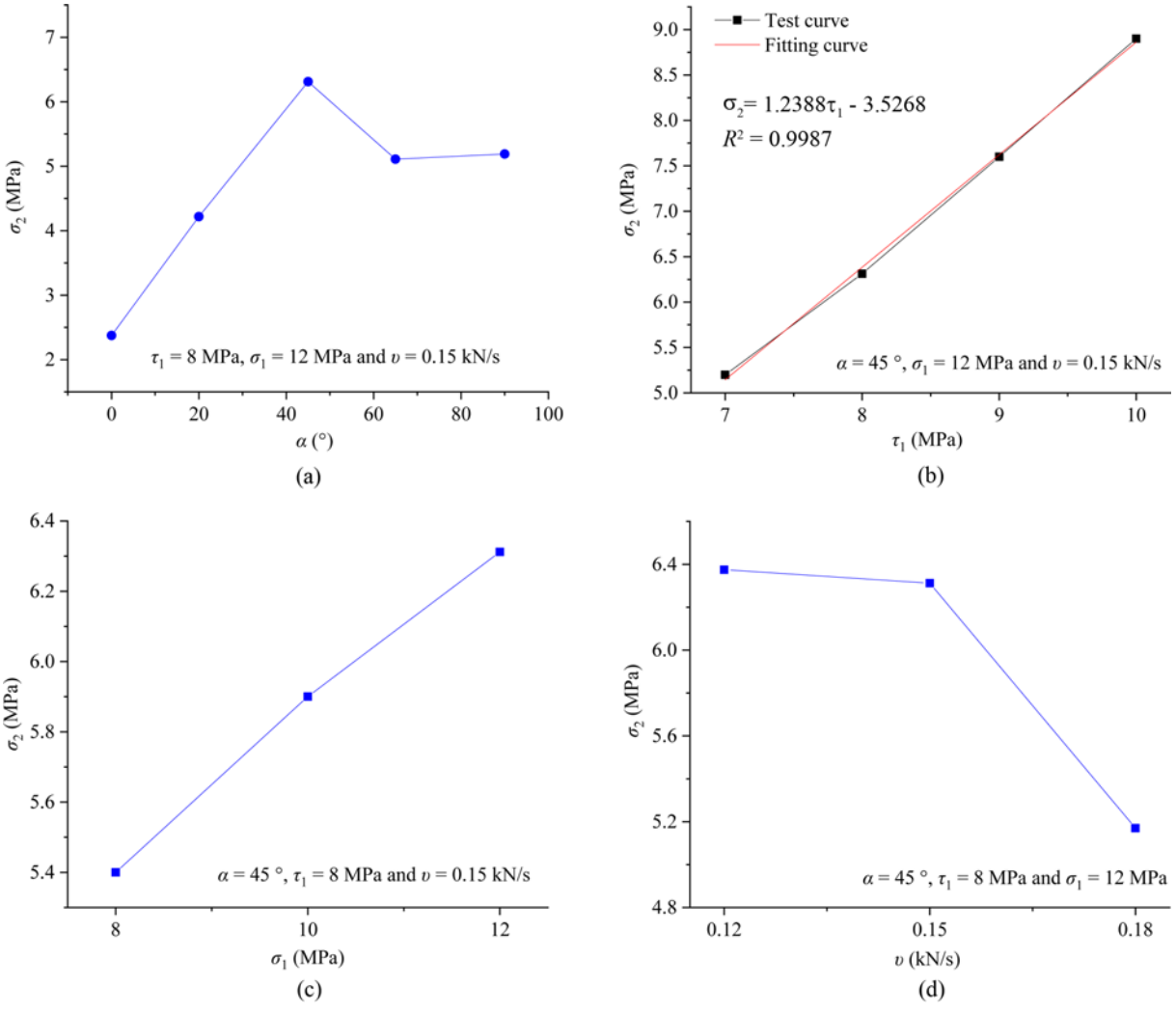

Fig. 11. Curves of the Failure Normal Stress (σ_2): (a) With Different Fissure Inclination, (b) With Different Initial Shear Stress, (c) With Different Initial Normal Stress, (d) With Different Normal Unloading Rate

= 45°) with the same initial stress level. On the whole, the failure normal stress (σ_2) decreases with the increase of the normal unloading rate (υ). And when the unloading rate is less than 0.15 kN/s, the decrease of σ_2 is slow, while the unloading rate increases from 0.15 kN/s to 0.18 kN/s, σ_2 decreases rapidly. This indicates that the shear strength of the specimens increases with the increase of unloading rate. This is because the normal shear expansion deformation will lag slightly when the normal unloading. And the larger unloading rate lead to the lag more obvious.

3.3 Deformation Characteristics

The typical displacement-time curve beginning at shear stress loading was shown in Fig. 12. The starting time and deformation of shear stress loading are recorded as 0 in Fig. 12. In the stage of shear loading, the normal stress remains unchanged. The horizontal displacement (X_disp)-time curve is convex, which indicates that the change rate is continuously decreasing. Meanwhile, due to the normal shear expansion effect, the vertical displacement

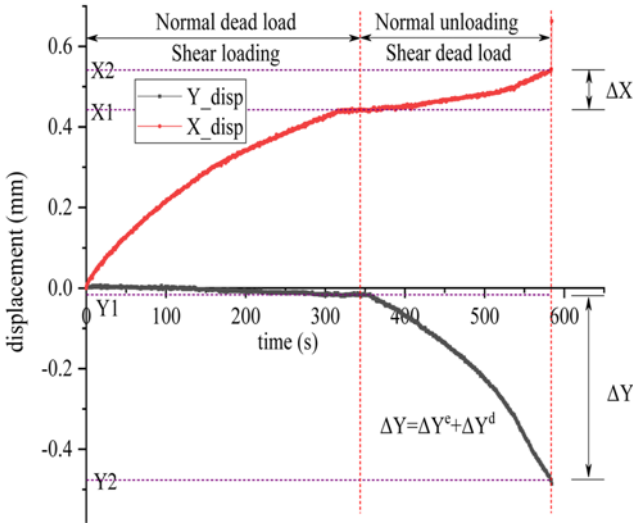

Fig. 12. Typical Displacement-Time Curves of the Specimens

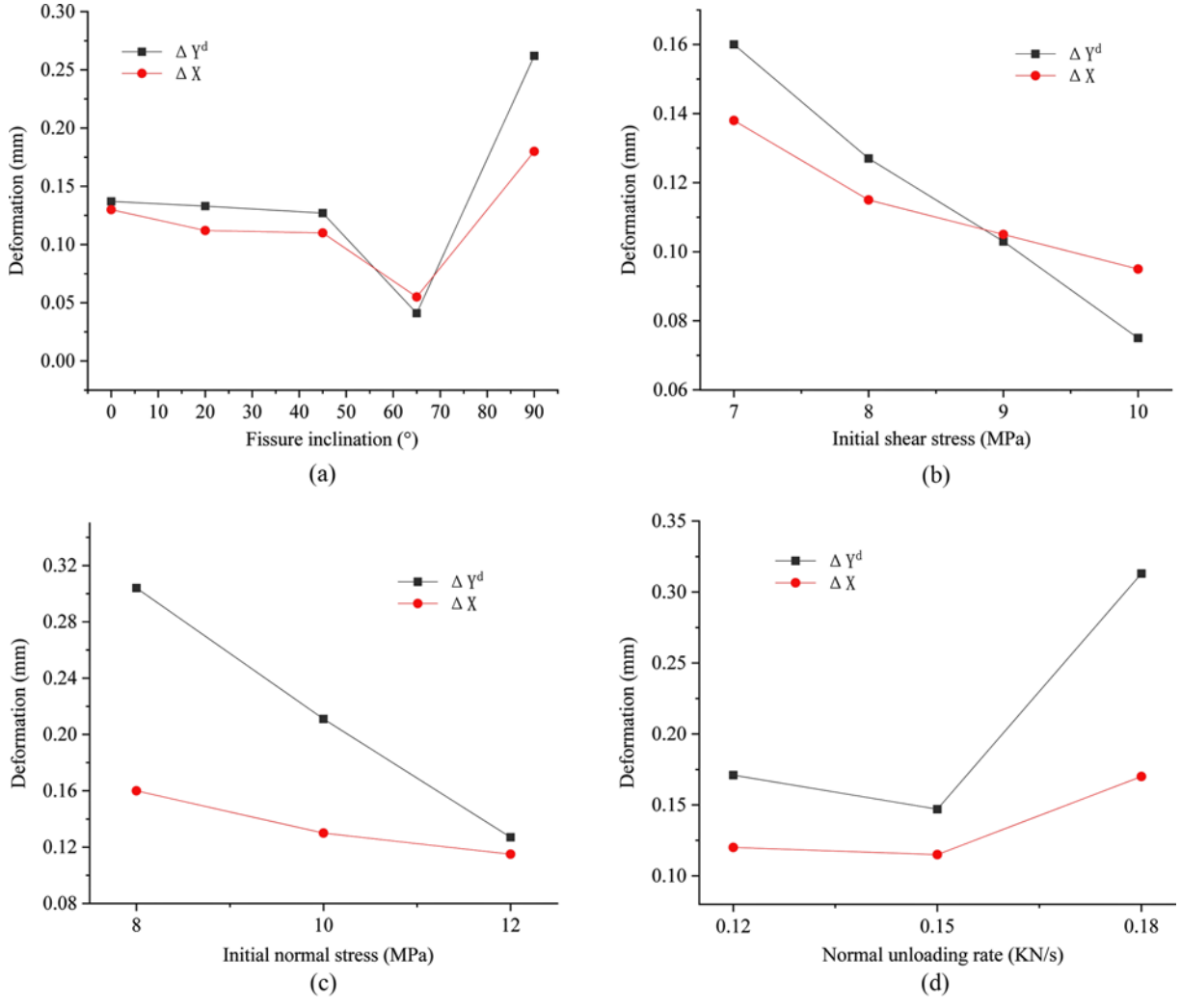

Fig. 13. Curves of the Vertical Dilatancy Deformation (ΔY^d) and Horizontal Shear Deformation (ΔX) in the Stage of Normal Unloading: (a) With Different Fissure Inclination (α), (b) With Different Initial Shear Stress (τ_1), (c) With Different Initial Normal Stress (τ_1), (d) With Different Unloading Rate (υ)

(Y_disp) decreases slightly. In the stage of normal unloading, the shear stress remains unchanged. X_disp and Y_disp keep increasing and decreasing respectively, and their change rate gradually increase until a displacement mutation occurs in both X_disp and Y_disp and the failure of the specimen takes place. The reason for the nonlinear change of the X_disp-time and Y_disp-time curves is that, in addition to the deformation of the rock itself, X_disp and Y_disp also include the slow deformation of the prefabricated fissure.

In Fig. 12, ΔY stands for the vertical deformation from initial normal unloading to the critical failure, which contains elastic deformation released by normal unloading and dilatancy deformation caused by shearing, termed as ΔY^e and ΔY^d, respectively, and ΔY^d is the component that significantly affects rock failure. Similarly, ΔX stands for the horizontal deformation from initial normal unloading to the critical failure. In order to further analyze the deformation characteristics of the normal unloading process, the curves of ΔX and ΔY^d with the change of the fissure inclination, initial shear stress, initial normal stress and normal unloading rate are obtained, as shown in Fig. 13.

It can be seen from Fig. 13(a) that with the change of the fissure inclination from 0° to 90°, ΔY^d and ΔX show a trend of increasing after decreasing, and the maximum value of ΔY^d and ΔX appear in

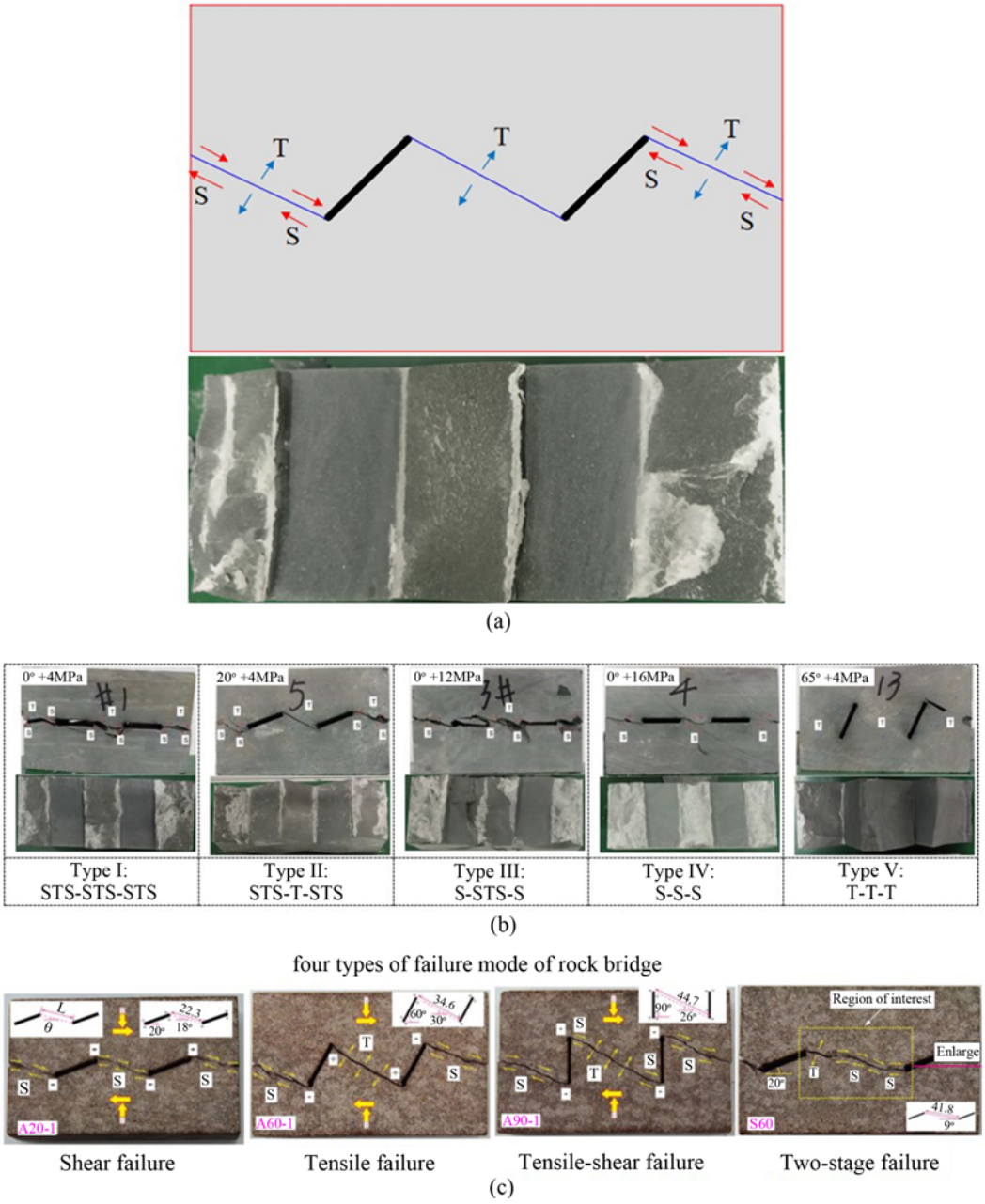

Fig. 14. Comparison of the Failure Modes Between Loading and Unloading and Those between the Current Study and Previous Studies: (a) Normal Unloading Shear Tests of Marlstone in This Study, (b) Direct Shear Tests of Marlstone (Yin et al., 2020), (c) Normal Unloading Shear Tests of Red-Sandstone (Zhong et al., 2020)

the fissure inclination of 65° which have the largest rock bridge dip. In addition, ΔY^d is slightly larger than ΔX (except for the fissure inclination of 65°). The curves of ΔY^d–α and ΔX–α present a "V" in shape, which is consistent with the results of Fig. 11(a).

Figure 13(b) shows the relationships between ΔY^d and τ_1, ΔX and τ_1. With the change of the initial shear stress from 7 MPa to 10 MPa, ΔY^d and ΔX show a trend of decreasing. This is because the ultimate failure shear deformation of the specimens is limited. Under the action of high initial shear stress, large shear displacement has taken place in the stage of shear loading. At the same time, it can be seen from Fig. 11(b) that with the increase of the initial shear stress (τ_1), the failure normal stress (σ_2) increases linearly, which leads to the stronger normal compaction effect. Therefore, with the increase of the initial shear stress, the horizontal deformation and normal deformation caused by shear effect decrease in the unloading stage. Moreover, under the action of low shear stress, ΔY^d is slightly larger than ΔX, and reverse when the initial shear stress increases to 9 MPa, which indicates that the increasing effect of high shear stress on ΔX is greater than that of ΔY^d.

It can be seen from Fig. 13(c) that with the change of initial normal stress (σ_1) from 8 MPa to 12 MPa, ΔY^d and ΔX show a trend of decreasing. This is due to that with the increase of σ_1, the failure normal stress increases (as shown in Fig. 11(c)), which leads to the stronger normal compaction effect. Therefore, with the increase of the initial normal stress, the horizontal deformation and normal deformation caused by shear effect decreases in the unloading stage. Besides, ΔY^d is significantly larger than ΔX. And with the increase of the initial normal stress, ΔY^d and ΔX are closer and closer, which means that the inhibiting effect of high normal stress on ΔY^d is greater than that of ΔX.

In Fig. 13(d), with the change of normal unloading rate from 0.12 kN/s to 0.15 kN/s, the change of ΔY^d and ΔX is not obvious, while significant increase with the change of normal unloading rate from 0.15 kN/s to 0.18 kN/s. It can be seen from Fig. 11(d) that this is also consistent with the change of the failure normal stress (σ_2). Furthermore, ΔY^d is significantly larger than ΔX.

4. Discussion

In this study, the effects of unloading normal stress on the shear mechanical behaviour of marlstone containing parallel fissures were investigated. The failure patterns and fracture mechanism, the strength and deformation behavior of rock specimens with different fissure inclinations under different initial stresses and unloading rates were analyzed. Fig. 11 shows the differences of the failure modes between loading and unloading and those between the current study and previous studies. In this study, the failure on the rock bridge is all tensile failure except for the limited extrusion failure at the tip of the prefabricated fissure (Fig. 11(a)). But in the direct shear tests of marlstone (Yin et al., 2020), three failure modes of the rock bridge were found: shear failure, tensile failure, and shear-tensile-shear failure (Fig. 11(b)). This shows that the tensile failure characteristics of rock bridge under unloading shear are more obvious. It can be explained by the perspective of deformation. In the direct shear tests, the normal stress remains unchanged, the shear stress increases continuously, and the deformation is mainly shear deformation, while in the unloading shear tests, the shear stress remains unchanged and the normal stress decreases, and the main deformation form is the release of normal elastic deformation. However, under the same test method (unloading shear tests), the results of Zhong et al. (2020) are quite different to this study, and four failure modes of shear failure, tensile failure, shear-tensile-shear failure, and two-stage failure were found in their study (Fig. 11(c)). The reason may be that the initial normal stress used in their study (20 MPa) is much larger than that in this study (12 MPa). And too high of normal stress may cause local damage to the specimens containing fissures. In addition, the mechanical properties of red sandstone are quite different from that of marlstone.

In addition to the fissure inclination and initial stress level, the mechanical properties of rock and the stress path also have great influence on the test results. The failure characteristics of the rock specimens are influenced by many factors. This study is mainly experimental research. In order to further understand the shear failure mechanism under normal stress unloading, numerical simulation method will be used for researching combined with experiment in the future. The phase field model (PFM) (Zhou et al., 2018a; Zhou et al., 2018b; Ren et al., 2019; Zhou et al., 2019; Zhuang et al., 2019) is one of the superior methods at present on this study, that will be a good future aspect for the current study.

5. Conclusions

The failure characteristics, strength and deformation properties of the specimens are significantly affected by the fissure inclination, initial stress level and unloading rate. The area of shear failure zone of the specimen decreases first and then increases with the increase of fissure inclination, increases with an increase in the initial shear stress/initial normal stress, and decreases with the increase of unloading rate. The failure on the rock bridge is tensile failure except for the limited extrusion failure at the tip of the prefabricated fissure. The failure on both sides is generally tensile-shear mixed failure, in which the tensile failure is mainly concentrated in the middle of both sides. In general, it can be summarized as a tensile-shear failure mode of STS-T-STS.

The failure normal stress gradually increases as the fissure inclination increases from 0° to 45°, and reverses when the fissure inclination grows from 45° to 90°. The failure normal stress increases linearly with the increase of the initial shear stress, increases slightly with the increase of the initial normal stress, and decreases with the increase of unloading rate. When the unloading rate is less than 0.15 kN/s, the failure normal stress decreases slowly, while the unloading rate increases from 0.15 kN/s to 0.18 kN/s, the failure normal stress decreases rapidly.

The variation law of the vertical dilatancy deformation and horizontal shear deformation in the stage of normal unloading is just opposite to that of the failure normal stress. Strong dilation

occurred in the shear process of the specimens, which shows obvious arch effect. The increasing effect of high shear stress on shear deformation is greater than that of dilatancy deformation, while the inhibiting effect of high normal stress on dilatancy deformation is greater than that of the shear deformation.

The failure characteristics of the rock specimens are influenced by many factors. This study is mainly experimental research. In order to further understand the shear failure mechanism under normal stress unloading, numerical simulation method will be used for researching combined with experiment in the future. The phase field model (PFM) is one of the superior methods at present on this study, that will be a good future aspect for the current study.

Acknowledgments

This work was supported by the National Key R and D Program of China (Grant No. 2018YFC1504802); the Fundamental Research Funds for the Central Universities (Grant No.2019CDXYTM0032); and the National Natural Science Foundation of China (Grant No. 41972266).

ORCID

Xinrong Liu https://orcid.org/0000-0003-2532-4709
Zhongping Yang https://orcid.org/0000-0002-2919-1395

References

Brideau M, Yan M, Stead D (2009) The role of tectonic damage and brittle rock fracture in the development of large rock slope failures. *Geomorphology* 103(1):30-49, DOI: 10.1016/j.geomorph.2008.04.010

Eberhardt E, Stead D, Coggan JS (2004) Numerical analysis of initiation and progressive failure in natural rock slopes — The 1991 Randa rockslide. *International Journal of Rock Mechanics and Mining Sciences* 41(1):69-87, DOI: 10.1016/S1365-1609(03)00076-5

GB/T 50266-2013 (2013) Standard for tests method of engineering rock masses. GB/T 50266-2013, China Planning Press, Beijing, China (in Chinese)

Gehle C, Kutter HK (2003) Breakage and shear behaviour of intermittent rock joints. *International Journal of Rock Mechanics and Mining Sciences* 40(5):687-700

Gratchev I, Kim DH, Yeung CK (2016) Strength of rock-like specimens with pre-existing cracks of different length and width. *Rock Mechanics and Rock Engineering* 49(11):4491-4496, DOI: 10.1007/s00603-016-1013-1

Guo S, Qi S (2015) Numerical study on progressive failure of hard rock samples with an unfilled undulate joint. *Engineering Geology* 193(1):173-182, DOI: 10.1016/j.enggeo.2015.04.023

Hoek E (1983) Strength of jointed rock masses. *Geotechnique* 33(3):187-223, DOI: 10.1680/geot.1983.33.3.187

Huang R (2008) Geodynamical process and stability control of high rock slope development. *Chinese Journal of Rock Mechanics and Engineering* 27(8):1525-1544, DOI: 10.3321/j.issn:1000-6915.2008.08.002 (in Chinese)

Huang R, Huang D (2014) Evolution of rock cracks under unloading condition. *Rock Mechanics and Rock Engineering* 47(2):453-466, DOI: 10.1007/s00603-013-0429-0

Huang R, Qi S (2017) Engineering geology: Review and prospect of past ten years in China. *Journal of Engineering Geology* 25(2):257-276, DOI: 10.13544/j.cnki.jeg.2017.02.001 (in Chinese)

Lajtai EZ (1969) Shear strength of weakness planes in rock. *International Journal of Rock Mechanics and Mining Sciences* 6(5):499-515, DOI: 10.1016/0148-9062(69)90016-3

Liu E (2012) Deformation mechanisms of crushable blocky materials upon lateral unloading for a biaxial stress state. *Rock Mechanics and Rock Engineering* 45(3):439-444, DOI: 10.1007/s00603-011-0210-1

Post G, Bonazzi D (1987) Latest thinking on the malpasset accident. *Engineering Geology* 24(5):339-353, DOI: 10.1016/0013-7952(87)90071-8

Ren HL, Zhuang XY, Anitescu C, Rabczuk T (2019) An explicit phase field method for brittle dynamic fracture. *Computers and Structures* 217(2019):45-56, DOI: 10.1016/j.compstruc.2019.03.005

Tang F (1989) Mechanism analysis of landslide by mining. *Journal of Xi'an Mining Institute* 3(3):32-36, DOI: 10.13800/j.cnki.xakjdxxb.1989.03.007 (in Chinese)

Terzaghi K (1962) Stability of steep slopes on hard unweathered rock. *Geotechnique* 12(4):251-270, DOI: 10.1680/geot.1962.12.4.251

Wong RHC, Leung WL, Wang SW (2001) Shear strength studies on rock-like models containing arrayed open joints. Proceedings of the 38th US symposium on rock mechanics (USRMS), July 7-10, Washington DC, USA

Wong R, Wang S (2002) Experimental and numerical study on the effect of material property, normal stress and the position of joint on the progressive failure under direct shear. Proceedings of the mining and tunneling innovation and opportunity, July 7-10, Toronto, ON, Canada

Xiao R, Chen H, Leng Y, Wei Y, Wang W (2018a) Preliminary analysis on the failure process and mechanism of the August 28 collapse in Nayong County, Guizhou Province. *The Chinese Journal of Geological Hazard and Control* 29(1):3-9, DOI: 10.16031/j.cnki.issn.1003-8035.2018.01.02 (in Chinese)

Xiao T, Huang M, Cheng C, He Y (2018b) Experimental investigation on the mechanical characteristics and deformation behaviour of fractured rock-like material with one single fissure under the conventional triaxial compression. *Shock and Vibration* 2018(2018):1-11, DOI: 10.1155/2018/2608639

Xie H Q, He C (2004) Study of the unloading characteristics of a rock mass using the triaxial test and damage mechanics. *International Journal of Rock Mechanics and Mining Sciences* 41(3):74-80, DOI: 10.1016/j.ijrmms.2004.03.022

Yang S, Jiang Y Z, Xu W, Chen X (2008) Experimental investigation on strength and failure behavior of pre-cracked marble under conventional triaxial compression. *International Journal of Solids and Structures* 45(17):4796-4819, DOI: 10.1007/978-3-662-47303-0_8

Yin Z, Liu X, Yang Z, Jiang Y, Zhao Y, Li S (2020) Shear characteristics and failure mode of hard brittle marl with parallel discontinuous structural plane. *Arabian Journal for Science and Engineering* 45:8219-8229, DOI: 10.1007/s13369-020-04674-5

Zhang J, Zhou X (2020) AE event rate characteristics of flawed granite: From damage stress to ultimate failure. *Geophysical Journal International* 222(2):795-814, DOI: 10.1093/gji/ggaa207

Zhang J, Zhou X, Zhou L, Berto F (2019) Progressive failure of brittle rocks with non-isometric flaws: Insights from acousto-optic-mechanical (AOM) data. *Fatigue and Fracture of Engineering Materials and Structures* 42(8):1787-1802, DOI: 10.1111/ffe.13019

Zhao Z, Jing H, Shi X, Han G (2019) Experimental and numerical study on mechanical and fracture behavior of rock-like specimens containing

pre-existing holes flaws. *European Journal of Environmental and Civil Engineering* 2:1-21, DOI: 10.1080/19648189.2019.1657961

Zhong Z, Huang D, Zhang Y, Ma G (2020) Experimental study on the effects of unloading normal stress on shear mechanical behaviour of sandstone containing a parallel fissure pair. *Rock Mechanics and Rock Engineering* 53(4):1647-1663, DOI: 10.1007/s00603-019-01997-0

Zhou S, Rabczuk T, Zhuang X (2018a) Phase field modeling of quasi-static and dynamic crack propagation: Comsol implementation and case studies. *Advances in Engineering Software* 122:31-49, DOI: 10.1016/j.advengsoft.2018.03.012

Zhou S, Zhuang X, Rabczuk T (2018b) A phase-field modeling approach of fracture propagation in poroelastic media. *Engineering Geology* 240:189-203, DOI: 10.1016/j.enggeo.2018.04.008

Zhou S, Zhuang X, Rabczuk T (2019) Phase field modeling of brittle compressive-shear fractures in rock-like materials: A new driving force and a hybrid formulation. *Computer Methods in Applied Mechanics and Engineering* 355:729-752, DOI: 10.1016/j.cma.2019.06.021

Zhuang X, Zhou S, Sheng M, Li G (2019) On the hydraulic fracturing in naturally-layered porous media using the phase field method. *Engineering Geology* 266:105306, DOI: 10.1016/j.enggeo.2019.105306